ISSN 1063-7826, Semiconductors, 2015, Vol. 49, No. 11, pp. 1483–1492. © Pleiades Publishing, Ltd., 2015.
Original Russian Text © V.G. Talalaev, B.V. Novikov, G.E. Cirlin, H.S. Leipner, 2015, published in Fizika i Tekhnika Poluprovodnikov, 2015, Vol. 49, No. 11, pp. 1531–1539.

SEMICONDUCTOR STRUCTURES, LOW-DIMENSIONAL SYSTEMS, AND QUANTUM PHENOMENA

Temperature Quenching of Spontaneous Emission in Tunnel-Injection Nanostructures

V. G. Talalaev[a,b]*, B. V. Novikov[a], G. E. Cirlin[c,d], and H. S. Leipner[e]

[a]*St. Petersburg State University, Fock Institute of Physics, Petrodvorets, 198504 Russia*
[b]*Martin Luther University Halle-Wittenberg, ZIK SiLi-nano, Halle, 06120 Germany*
[c]*Academic University, Nanotechnology Center, Russian Academy of Sciences, St. Petersburg, 194021 Russia*
[d]*Institute of Analytical Instrument Design, Russian Academy of Sciences, St. Petersburg, 190103 Russia*
[e]*Martin Luther University Halle-Wittenberg, ICMS, Halle, 06120 Germany*
** e-mail: vadimtalalaev@yandex.com*

Submitted April 13, 2015; accepted for publication April 20, 2015

Abstract—The spontaneous-emission spectra in the near-IR range (0.8–1.3 μm) from inverted tunnel-injection nanostructures are measured. These structures contain an InAs quantum-dot layer and an InGaAs quantum-well layer, separated by GaAs barrier spacer whose thickness varies in the range 3–9 nm. The temperature dependence of this emission in the range 5–295 K is investigated, both for optical excitation (photoluminescence) and for current injection in *p–n* junction (electroluminescence). At room temperature, current pumping proves more effective for inverted tunnel-injection nanostructures with a thin barrier (<6 nm), when the apexes of the quantum dots connect with the quantum well by narrow InGaAs straps (nanobridges). In that case, the quenching of the electroluminescence by heating from 5 to 295 K is slight. The quenching factor S_T of the integrated intensity I is $S_T = I_5/I_{295} \approx 3$. The temperature stability of the emission from inverted tunnel-injection nanostructures is discussed on the basis of extended Arrhenius analysis.

DOI: 10.1134/S1063782615110214

1. INTRODUCTION

The development of optoelectronics relies on new light-emitting devices with distinctive properties: miniature size, low energy consumption, a bright emission spectrum that may be tuned, temperature stability, and noise resistance. Of particular interest are semiconductor quantum-dot nanostructures, which meet several of those requirements [1]. However, the prospects for quantum-dot systems as temperature-independent active elements have been exaggerated [2, 3]. Therefore, the emission of quantum-dot systems with a δ-type spectrum are currently being studied with a view to the creation of single-photon emitters based on individual quantum dots [4, 5].

Another problem of light-emitting quantum-dot systems is pumping. On the one hand, the capture cross section of quantum dots in the direct excitation of their ground states is small. On the other, the pumping of quantum dots by hot carriers in matrix and/or in wetting layer leads to the parasitic influence of excited states [3]. This may be addressed by adding a quantum-well layer to the quantum-dot system, in a tunnel vicinity of the quantum-dot layer. These are known as tunnel-injection structures with quantum dots [6]. Tunnel-injection quantum-dot lasers have a forward sequence of layers in the direction of growth [7]: quantum well–barrier–quantum dot. Spatial separation of the carrier injector (the quantum well) and the light nanoemitter (the quantum dot) ensures a new degree of freedom in the design of the lasers' active region: the possibility of tuning the energy spectra of the quantum well relatively quantum dot. The tunneling of cold carriers from the quantum well to the ground state of the quantum dot significantly reduces the internal losses and diffusional capacity and increases the speed and differential efficiency of the laser diodes. However, the threshold current of tunnel-injection quantum-dot lasers (180 A cm^{-2}) [8] cannot match that of lasers with quantum-dot-in-quantum-well structure (40 A cm^{-2} for two dot–well layers) [9]. Obviously, this deficiency of tunnel-injection quantum-dot lasers is associated with the tunnel constraints on the carrier transfer from the injector (the quantum well) to the light emitter (the quantum dot).

In the present work, we consider an inverted tunnel-injection nanostructure consisting of an InGaAs quantum dots, a GaAs barrier, and an InGaAs quantum well, as in [10–13]. Inversion of the nanolayers retains all the benefits of a traditional (forward) tunnel-injection structure. Thanks to the larger capture cross section and the stepwise state density, the quantum well again acts as an effective carrier store, while the injection of cold carriers directly populates the

ground states of the quantum dot participating in radiative recombination. The efficiency of carrier transfer from the quantum well to the quantum dot is unexpectedly improved in such structures. Inversion of the nanolayers leads to quasi-point contacts (nanobridges) between the apexes of the quantum dots and quantum well separated by a thin barrier. The nanobridges eliminate this barrier and accelerate carrier injection from the quantum well to the quantum dot. That removes the limit on the flow density of the carriers associated with exponential tunnel transport. This deviation from the quasi-classical Wentzel–Kramers–Brillouin approximation not only eliminates the exponential constraint on the rate of carrier tunneling from the quantum well to the quantum dot (immediate injection through the nanobridge) [10, 11] but also permits control of the number of active quantum dots [14, 15]. That offers the possibility of creating a single-photon emitter on the basis of an inverse tunnel-injection nanostructure. The size dispersion of the quantum-dot structure is fundamental importance here. The nanobridges are formed at the largest quantum dots and are characterized by dispersion with respect to the length [13, 14, 16]. Short InGaAs nanobridges (less than 2 nm) do not contain hole eigenstates and do not lead to immediate carrier injection from the quantum well to the quantum dot. As a result, the number of active nanobridges is reduced. In addition, short nanobridges may be burned out by a pulsed current of specific amplitude in *p*–*n* junction [14, 15].

In the present work, we investigate the efficiency of an inverse tunnel-injection nanostructure with quantum dots as a near-IR emitter in terms of the temperature stability of its spontaneous-emission spectrum.

The temperature dependence of semiconductor quantum dots has been systematically investigated with a view to creating room-temperature lasers in the visible and near-IR ranges [17–21]. Anomalies in the temperature dependence of the luminescence spectra always require careful study [20–23]. Nevertheless, the interpretation of experimental data is often contradictory. One unresolved question, for example, is the role of the wetting layer in the temperature dependence of the emission spectra of quantum dots in adjacent layers separated by barrier [20, 24]. Despite the complexity of the kinetic model of relaxation, capture, redistribution, and recombination of carriers in the quantum-dot system, temperature quenching of the luminescence is still regarded as a process of thermal electron and/or hole ejection from the ground level in the potential well of the quantum dot to the barrier-layer continuum [18, 25–27]. In that case, the temperature dependence of the integrated intensity of the emission band may be described by the Arrhenius equation

$$I(T) = \frac{I_M}{1 + C_F \exp\left(-\frac{E_A}{kT}\right)}, \qquad (1)$$

where I_M is the maximum intensity (usually at low temperature); C_F is a dimensionless constant determined by the position of the Fermi level [28] and/or by the ratio of the exciton lifetime in the quantum dot to its scattering time on the interface with the barrier [29]. In Eq. (1), the temperature dependence of C_V is usually neglected in comparison with the exponent $\exp\left(-\frac{E_A}{kT}\right)$. Here E_A is the activation energy of the state—that is, the energy gap between the ground level in the quantum dot and the barrier. Thus, Arrhenius analysis may be a powerful tool for the construction of energy and kinetic models of semiconductor nanostructures.

2. EXPERIMENT

Two types of experimental InGaAs/GaAs inverse tunnel-injection nanostructures with a quantum-dot–quantum-well tunnel pair are grown by molecular-beam epitaxy. The first type is intended for the investigation of the photoluminescence and includes only semiinsulating layers without special doping. After the deposition of a GaAs buffer layer on the GaAs (100) substrate, a limitative three-period $Al_{0.25}Ga_{0.75}As$ (2.5 nm)/GaAs (2.5 nm) *SL*1 superlattice and then a GaAs layer (thickness 20 nm) are grown. Then the substrate temperature is reduced from 550 to 485°C and an active region is formed by deposition of two InAs monolayers for the quantum dots (Stranski-Krastanov mode), a GaAs barrier layer, and an $In_{0.15}Ga_{0.85}As$ quantum well (thickness 11 nm) (Fig. 1a). The barrier thickness B varies from 3 to 9 nm. In the final stage, the substrate temperature rises to 550°C, and the upper set of layers is grown, symmetrically with the lower layer set.

The second type of structure is intended for the study of electroluminescence. For this aim, the active region between the limitative superlattices *SL*1 and *SL*2 remains undoped, while the outer layers are doped: the buffer layer and *SL*1, like the substrate, are of *p* type, while *SL*2 and the contact cap layer are of *n* type. The level of doping is 5×10^{18} cm^{-3}. Thus, such inverse tunnel-injection nanostructures consist of an active *i* region with quantum-dot–barrier–quantum-well layers built into the *p*–*n* junction.

Injection for electroluminescence is stimulated by current pumping at a forward bias on the *p*–*i*–*n* structure. A mesa structure M (diameter 1.4 mm) is created by photolithography and reactive ion–plasma etching; its base is a *p*-type buffer layer (Fig. 1b). Ohmic con-

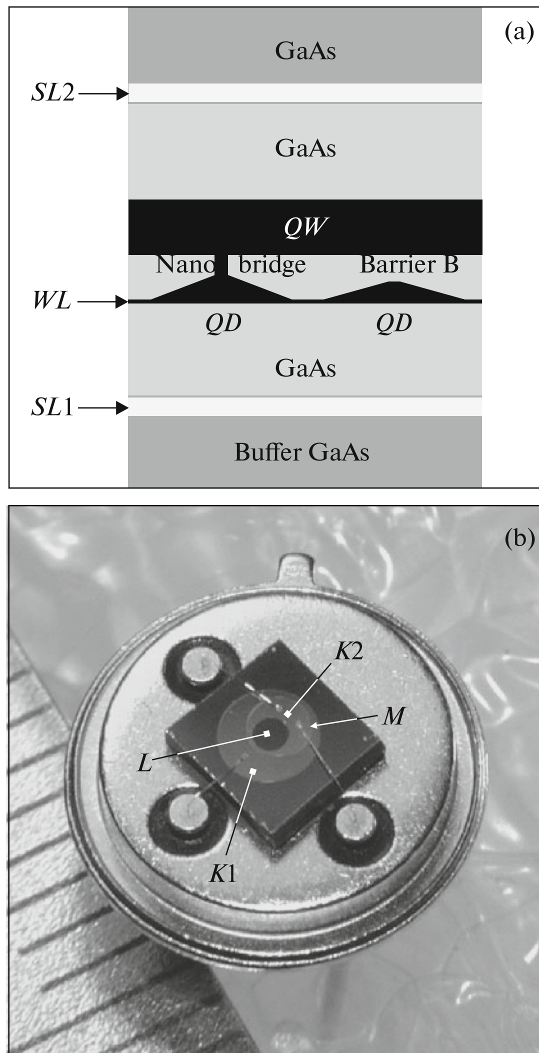

Fig. 1. (a) Basic configuration of the inverse tunnel-injection nanostructures of quantum-dot–barrier–quantum-well type (at the right) and quantum-dot–nanobridge–quantum-well type (at the left); (b) a light-emitting diode, in the form of a chip with an inverse tunnel-injection nanostructure (a mesa structure with contacts within the housing).

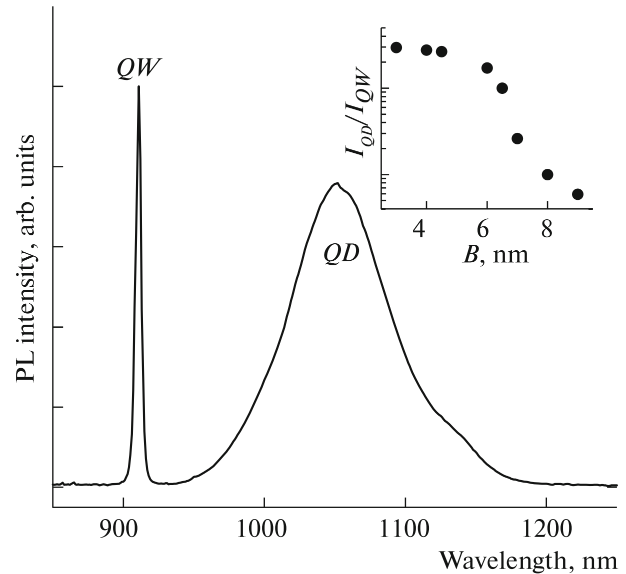

Fig. 2. Photoluminescence spectrum of the inverse tunnel-injection nanostructure with a thick barrier ($B = 8$ nm) at $T = 5$ K. Inset: intensity ratio I_{QD}/I_{QW} of the low-temperature photoluminescence of the *QD* and *QW* as a function of the barrier thickness *B* (experimental data).

tacts are applied by thermal sputtering in vacuum and are formed as plane rings by photolithography. The lower ring *K*1 in the *p*-type layer (external diameter 2.2 mm) is based on gold–zinc eutectic; the upper ring *K*2 in the *n*-type layer is based on gold–germanium eutectic. The internal diameter of this ring (0.8 mm) forms the output window *L* of the light emitter. Both eutectic layers are reinforced by gold (thickness 100 nm), and then the contacts are annealed at 400°C. The chip with mesa structure is soldered in a TO-39 housing by means of gold wire (Fig. 1b).

An Innova-308 Coherent argon laser (wavelength 488 nm) is used for the excitation of steady-state photoluminescence. The excitation density is 18 W cm^{-2}. The Thorlabs ITC-4005 source is used for the excitation of electroluminescence. The current density is maintained at 9 A cm^{-2}. That corresponds to an electric power density of 18 W cm^{-2}. The emission from the inverse tunnel-injection nanostructure is collected at the entrance slit of an Acton SpectraPro monochromator (focal length 0.5 m) by means of mirror optics. Beyond the monochromator, the luminescence spectrum is recorded by a cooled linear OMA-V InGaAs matrix (Princeton Instruments).

To investigate the temperature dependence of the photoluminescence and electroluminescence in the range 5–295 K, the samples are placed in a Konti CryoVac continuous-flow helium optical cryostat. The precision of temperature stabilization in the experiments is 0.5 K.

3. EXPERIMENTAL RESULTS

Measurements of the inverse tunnel-injection nanostructure by transmission electron microscopy show that the quantum dots take the form of a truncated cone (base diameter 180 nm, vertex diameter 2 nm, height 4 nm) and contain 60% indium ($x = 0.6$). The quantum dots lie on the InAs wetting layer (*WL* in Fig. 1a) with density 5×10^{10} cm^{-2}. The spectrum of the low-temperature photoluminescence (Fig. 2) reflects recombination between the ground states of the individual components within the inverse tunnel-injection nanostructure: the $In_{0.6}Ga_{0.4}As$ quantum dot

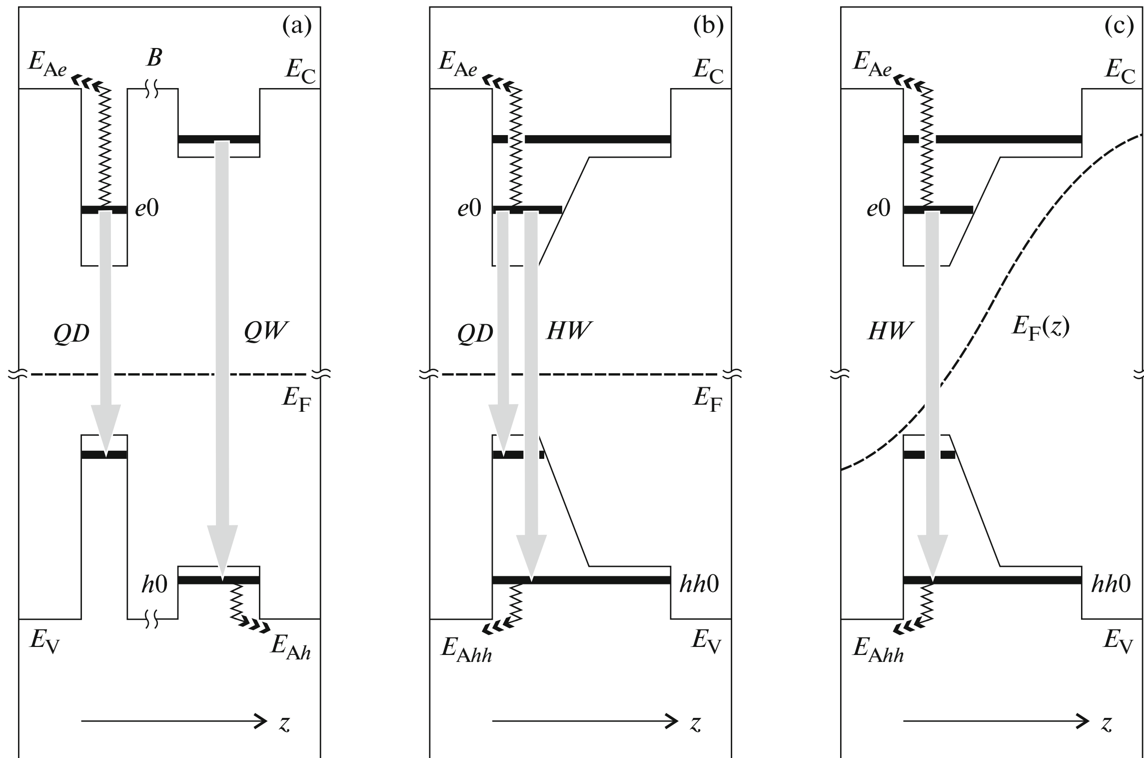

Fig. 3. Energy levels of structures with radiative transitions *QD*, *QW*, *HW* and thermal ejections E_{Ae}, E_{Ah}, E_{Ahh} for reference quantum dots and quantum well or an inverse tunnel-injection nanostructure with a thick barrier $B > 6$ nm (a) and an inverse tunnel-injection nanostructure with a thin barrier $B < 6$ nm and a hybrid well *hh*0 in the case of weak photoexcitation (b) and weak current pumping at positive bias on the *p–n* junction (c); E_F is the Fermi level or quasi-Fermi level for holes in the non-equilibrium case of weak excitation.

(a broad band *QD* centered close to 1050 nm); and the $In_{0.15}Ga_{0.85}As$ quantum well (a narrow line *QW* at 910 nm). The intensity ratio I_{QD}/I_{QW} increases with decrease in thickness *B* of the GaAs barrier from 9 to 3 nm, on account of the increase in the contribution of carrier tunneling from the quantum well to the quantum dot (Fig. 2, inset). This reflects the pumping principle of the light emitter (quantum dot) in the tunnel-injection structures.

First we investigate the radiative properties of reference structures grown with only one component: a quantum dot or a quantum well. For example, according to photoluminescence measurements (Hamamatsu streak-camera; time resolution 10 ps; 100-fs pulsed excitation) the exciton lifetime is $\tau_0 = 750$ ps in the single quantum dots and $\tau_0 = 420$ ps in a single quantum well [10].

Arrhenius analysis of the temperature dependence of the photoluminescence spectra for the reference structures yields the activation energy of the ground states in the quantum well and quantum dot, which are compared with calculations within the framework of effective-mass approximation for a quantum well (thickness 11 nm; $x = 0.15$) and a quantum dot in the form of a truncated cone (base diameter 180 nm, apex diameter 2 nm, height 4 nm; $x = 0.6$). On that basis, we derive the energy levels of the inverse tunnel-injection nanostructure (Fig. 3a). The table presents the activation energy E_A of the ground states for the carriers whose thermal escape is determined by the Arrhenius plot in the relevant temperature range. The first and second rows of the table correspond to the reference structures with a single quantum well and a single layer of quantum dots, respectively. These results are analyzed in the next section.

In the present work, we are most interested in the temperature dependence of the emission spectrum for an inverse tunnel-injection nanostructure with a quantum-dot–quantum-well tunnel pair. In Fig. 4, we show the Arrhenius plot in the initial coordinates of I/I_M and *T* for an inverse tunnel-injection nanostructure with a thick barrier ($B = 8$ nm) in the case of the quantum dot (*QD*) and quantum well (*QW*). The dotted curves correspond to fitting of the Arrhenius plot (*1*) to the experimental data. Note that Eq. (1) does not provide a satisfactory description of these data. Accordingly, another exponential term is added to the denominator of the Arrhenius equation to

Values of the activation energy E_A (meV) of the ground states, the coefficient C_F, and the quenching factor S_T calculated from Eq. (2) for various components of the inverse tunnel-injection nanostructure determining the temperature quenching the corresponding bands in the emission spectrum (the E_A values, meV, obtained from the Schrödinger equation are given in parentheses)

No.	Component	E_{Ae}	E_{Ah}	C_{Fe}	C_{Fh}	$S_T = I_5/I_{295}$
1	Photoluminescence band *QW*—a single quantum well	– (95)	90 (90)	–	300	22
2	Photoluminescence band *QD*—a single layer of quantum dots	210 (219)	– (295)	362 000	–	12
3	Photoluminescence band *QW*—a quantum well in an inverse tunnel-injection nanostructure with $B = 8$ nm	– (95)	55 (90)	–	16 800	1500
4	Photoluminescence band *QD*—quantum dots in an inverse tunnel-injection nanostructure with $B = 8$ nm	199 (219)	– (295)	23 500	–	11
5	Photoluminescence band *HW*—a hybrid quantum well in an inverse tunnel-injection nanostructure with $B = 4$ nm	–	104 (105)	–	12 100	1363
6	Electroluminescence band *HW*—a hybrid quantum well in an inverse tunnel-injection nanostructure with $B = 4$ nm	–	64 (105)	–	25	3

account for a secondary thermally stimulated process, in accordance with [28, 30]. Thus, we write

$$\frac{I(T)}{I_M} = \frac{N}{1 + C_F \exp\left(-\frac{E_A}{kT}\right) + C'_F \exp\left(-\frac{E'_A}{kT}\right)}. \quad (2)$$

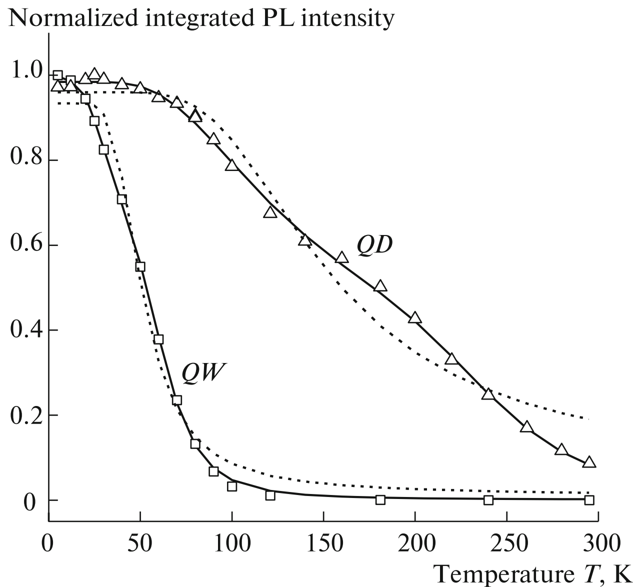

Fig. 4. Temperature dependence of the normalized integrated intensity I/I_M for the quantum dots (*QD*) and quantum well (*QW*) in an inverse tunnel-injection nanostructure with a thick barrier ($B = 8$ nm): the dashed curves correspond to fitting by means of Eq. (1) and the continuous curves to refined fitting by means of Eq. (2).

The secondary process is characterized by activation energy E'_A and coefficient C'_F. The numerator N is a fitting parameter and is close to one.

We find that Eq. (2) provides a very accurate description of the experimental temperature dependence of I/I_M for the inverse tunnel-injection nanostructure. In Fig. 4, the continuous curves corresponds to fitting of the experimental points by means of Eq. (2) when $B = 8$ nm. The corresponding E_A, C_F, and S_T values are presented in rows 3 and 4 of the table. Accordingly, we use Eq. (2) for the analysis of all the cases in the table. Note that the secondary process included in Eq. (2) is characterized by small values of the activation energy $E'_A = 8–24$ meV and $C'_F = 4–7$ in all cases and may be regarded as thermal dissociation of the exciton within the given component of the inverse tunnel-injection nanostructure [31].

On switching to a thinner barrier ($B < 6$ nm), the photoluminescence spectrum of the inverse tunnel-injection nanostructure changes, as we see in Fig, 5a ($B = 4$ nm). The intensity of the *QW* band is negligible. The new *HW* band appears at 1020 nm. The thermal quenching of this band and the extended Arrhenius analysis are shown in Fig. 5b. The E_A, C_F, and S_T values obtained by fitting for the *HW* band are shown in row 5 of the table.

Current pumping at a direct bias on inverse tunnel-injection nanostructure ($B = 4$ nm) in a *p–n* junction modifies the emission spectrum, as we see in Fig. 6a for $T = 5$ K (curve *1*). The component *QD* disappears from the electroluminescence spectrum. At room temperature, the electroluminescence is not signifi-

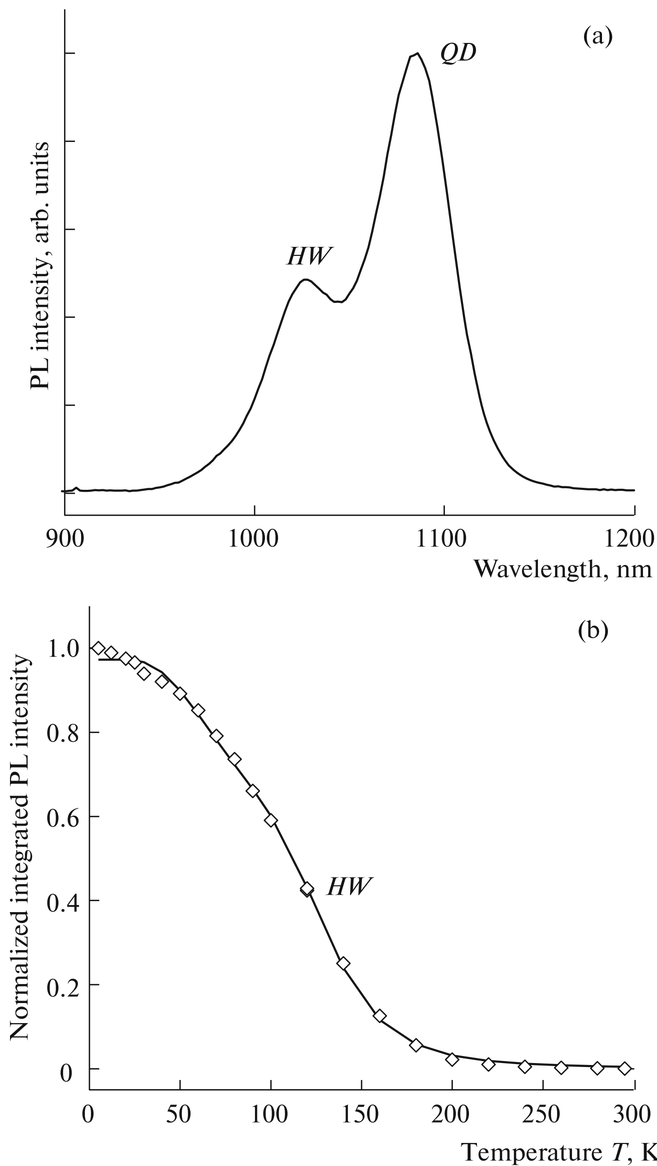

Fig. 5. (a) Photoluminescence spectrum of inverse tunnel-injection nanostructure with a thin barrier ($B < 6$ nm) at $T = 5$ K; (b) temperature dependence of the normalized integrated intensity I/I_{M} of the photoluminescence band *HW* and its extended Arrhenius analysis on the basis of Eq. (2).

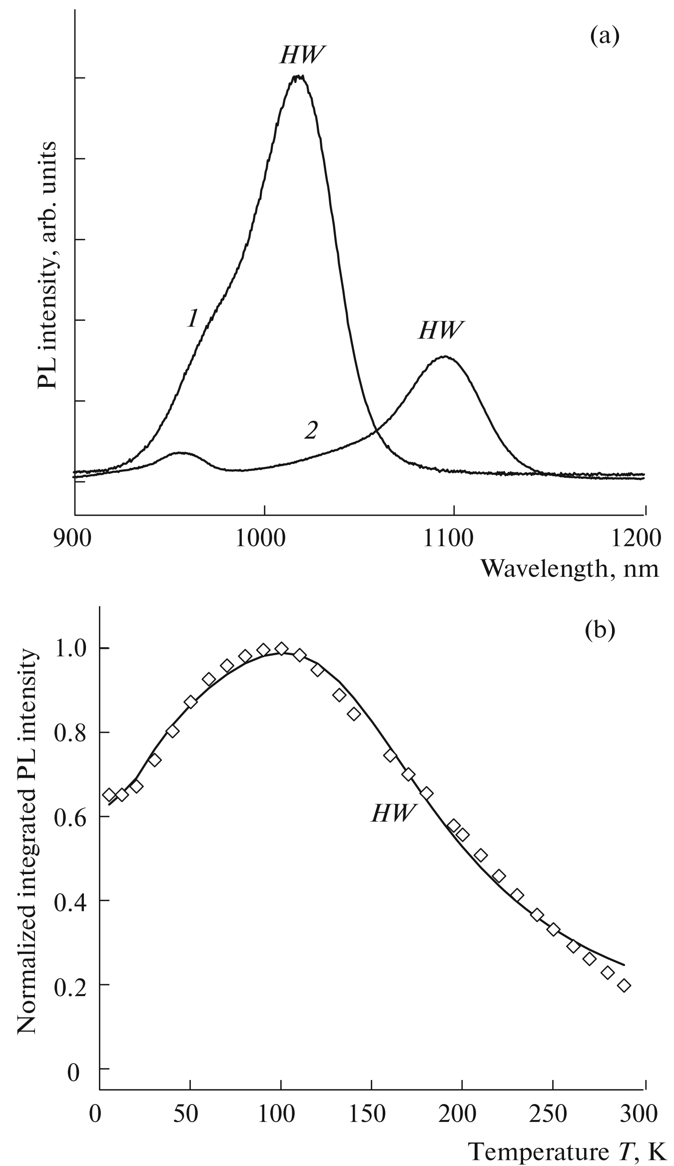

Fig. 6. (a) Electroluminescence spectrum in the case of current pumping of an inverse tunnel-injection nanostructure with a thin barrier ($B < 6$ nm) built into a *p–n* junction at $T = 5$ K (*1*) and 295 K (*2*); (b) temperature dependence of the normalized integrated intensity I/I_{M} of the photoluminescence band *HW* and its extended Arrhenius analysis on the basis of Eq. (2).

cantly different (Fig. 6a, curve *2*). In analysis of the temperature dependence of the *HW* band (Fig. 6b), we note the initial increase of *HW* intensity in the range 5–100 K. As follows the table (row 6), a very low value $S_T = 3$ is obtained, despite the lowering the barrier under current pumping (64 meV, instead of 104 meV for optical pumping), while C_{F} is 25.

4. DISCUSSION OF THE TEMPERATURE DEPENDENCE

The parameters obtained by Arrhenius analysis for an isolated quantum well (row 1 in the table) correspond to a simple physical model. The activation energy of the hole state may be described by the effective-mass approximation ($E_{\mathrm{A}h} = 90$ meV). From the values of $C_{\mathrm{F}} = \tau_0/\tau_s = 300$ and the exciton lifetime in the quantum well ($\tau_0 = 420$ ps), we may estimate the hole-scattering time at the InGaAs/GaAs interface as $\tau_s = 1.4$ ps. That corresponds to literature data [32].

For single quantum dots, the thermal quenching of the photoluminescence is determined by the thermal activation of an electron with energy $E_{\mathrm{A}e} = 210$ meV

(row 2 in the table). The slight discrepancy with the theoretical value (219 meV) may be attributed more to the imprecision of the model than to reduction of the barrier due to the InAs wetting layer. Since the potential well is deeper for the quantum dots than for the quantum well, S_T for the *QD* band is about half that for a single *QW*. Given the exciton lifetime in the quantum dot (τ_0 = 750 ps), we may conclude on the basis of the large value C_F = 36 200 that electron scattering at the interface between the quantum dots and the matrix is fast (tens of fs) due to the roughness of the interface formed by facets of the quantum dots.

Rows 3 and 4 in the table show that the parameters of the components here may be determined from the temperature quenching of the photoluminescence in the quantum-dot–barrier–quantum-well system of the inverse tunnel-injection nanostructure if the barrier thickness does not ensure effective carrier injection from the quantum well to the quantum dot (B = 8 nm). We see that the activation energies of electrons from the quantum dots and especially holes from the quantum well decline to E_{Ae}= 199 meV and E_{Ah} = 55 meV. In other words, the barrier height is reduced for both components. This may be due to the appearance of a thermostimulated potential difference at the barrier layer on account of the thermal escape of electrons from the quantum dots and holes from the quantum well. As a result of Coulomb interaction, the potential barriers for the electrons and holes are reduced. Since the probability of tunneling through the barrier is described by an exponential function in the quasi-classical Wentzel–Kramers–Brillouin approximation

$$W \propto \exp\left[-\frac{2B}{\hbar}\sqrt{2m_B^* E_A}\right], \qquad (3)$$

where m_B^* is the effective carrier mass in the barrier, this effect leads to the tunnel transfer of light electrons from the quantum well to the quantum dot. In other words, the system begins to operate as an inverse tunnel-injection nanostructure. This explains the almost fivefold increase in S_T for the quantum well and the slight decrease in S_T for the quantum dots. At the same time, we see significant increase in C_F to 16800 for the quantum well. As shown by electron microscopy, the relief of the quantum dot array is reproduced through the GaAs barrier on the walls of the quantum well, which are roughened.

Before discussing the temperature quenching of the spontaneous emission in an inverse tunnel-injection nanostructure with a thin barrier, we note the results for such structures in [10–14]. In an inverse tunnel-injection nanostructure with a thin GaAs barrier (B < 6 nm) between the InGaAs quantum-dot layer and quantum well, nanobridges are observed between the apexes of the quantum dots and quantum well. These are narrow channels (2 nm) enriched with indium. The nanobridges are formed at the apexes of the quantum dots under the influence of elastic stress, which results in the diffusion of indium atoms during growth. The nanobridges lead to local disappearance of the barrier and consequently to anomalously rapid carrier transfer from the injector (the quantum well) to the light emitter (the quantum dot). In the presence of nanobridges, the transfer time deviates from the quasi-classical Wentzel–Kramers–Brillouin approximation. That removes the exponential limitation on the flow density of the carriers associated with tunnel transfer in Eq. (3).

In terms of energy structure, an integrated region of dimensional quantization is formed in such inverse tunnel-injection nanostructures: a composite (or hybrid) potential well with a common system of levels. This system is described by volume-element solution of the three-dimensional Schrödinger equation, with Dirichlet boundary conditions, in a cylindrical coordinate system [33]. The calculations are conducted for a structure consisting of $In_{0.6}Ga_{0.4}As$ quantum dots in the form of a truncated cone (base diameter 18 nm, apex diameter 2 nm, height 4 nm), an InGaAs nanobridge (diameter 2 nm) with an indium gradient $0.6 > x > 0.15$, and an $In_{0.15}Ga_{0.85}As$ quantum well. The length of the nanobridge varies from 1 to 10 nm. The calculated E_{Ahh} values are presented in rows 5 and 6 of the table.

Since the quantum dots and nanobridges occupy only a small part of the hybrid system, its energy is mainly determined by the parameters of the initial unperturbed InGaAs quantum well (thickness 11 nm). However, the theoretical finding that a nanobridge longer than 2 nm has own hole eigenstates perturbs the hole subsystem. The density of the ground hybrid state *hh*0 in the valence band is distributed along the z axis over the whole thickness of the inverse tunnel-injection nanostructure.

In contrast to the heavy holes, electron eigenstates are impossible in a nanobridge of length less than 10 nm [16]. Therefore, the electron subsystem does not react strongly to the appearance of the nanobridge. The system of electron levels in the hybrid well corresponds to the initial components (the quantum dots and the quantum well), but there is not barrier between them. In these conditions, we note immediate carrier injection from the quantum well to the quantum dot. If we consider the wave functions of the final states between which transitions may appear in the emission spectrum of the quantum-dot–nanobridge–quantum-well system, the most likely outcome is transition between the electron ground state *e*0 of the quantum dots and the hole state *hh*0 of the hybrid well (Fig. 3b), on account of the fast relax-

ation of the electrons to the ground level of the quantum dots [32]. Radiative recombination between these states forms the new band *HW* in the spontaneous-emission spectra of the inverse tunnel-injection nanostructure with $B = 4$ nm (Figs. 5a and 6a). The oscillator strength of this transition is large, since the wave functions of the electrons in the quantum dots and the holes in the hybrid well significantly overlap.

We assume that, at low temperatures, the entire exciton is transferred from the quantum well to the quantum dots in an inverse tunnel-injection nanostructure with nanobridges, without an intermediate indirect-exciton state, since the strong-binding condition is satisfied for the two potential wells [34]. The transfer time derived from analysis of the time-resolved photoluminescence profiles is reduced to the time resolution limit [11]. With increase of temperature and transition to single-particle transfer due to the thermal dissociation of the excitons, this situation will be retained if the length of the nanobridge permits the existence of intrinsic eigenstates,—that is, if a hybrid well is formed. In cases where there are no nanobridges ($B > 6$ nm) or only short nanobridges ($B < 2$ nm), carrier transfer will be slow. On account of the difference in tunneling rates of the electrons and heavy holes, the transfer of the excitation from the quantum well to the quantum dots is limited by the holes. For double quantum wells, this is known as filtration by effective masses [35]. Although the appearance of Coulomb interaction lowers the barrier, the transfer of the excitation is slowed in an inverse tunnel-injection nanostructure without a hybrid well on account of the large hole mass, which exceeds the normalized exciton mass.

What is the effect of increasing the temperature on the emission properties of an inverse tunnel-injection nanostructure with a hybrid well? Are the benefits of spontaneous emission of an inverse tunnel-injection nanostructure with a thin barrier retained at room temperature? The dependence of the intensity ratio I_{QD}/I_{QW} on the barrier thickness (inset in Fig. 2) correlates with the corresponding dependence of the rate of exciton transfer from the quantum well to the quantum dots at low temperatures [13]. This is associated with competition between tunneling from the quantum well and radiative recombination within the quantum well ($\tau_0 = 420$ ps). The reduction in the transfer time τ_T with decrease in the barrier thickness B favors tunneling. However, at room temperature, another process competes with exciton transfer: thermal escape of carriers from the hybrid well.

As follows from the Arrhenius plot for an inverse tunnel-injection nanostructure with $B = 4$ nm (row 5 in the table), the photoluminescence intensity falls by more than three orders of magnitude ($S_T = 1363$), while the activation energy $E_{Ahh} = 104$ meV corresponds to the calculated value (105 meV) and $C_F = 12100$. In other words, E_A is higher, while C_F is lower, than when $B = 8$ nm; there are no nanobridges; and no hybrid well is formed (row 3). This may simply mean that our use of the Arrhenius formalism for the hybrid well quantum dot—nanobridge—quantum well is incorrect. However, that only affects C_F, which no longer retains its previous significance ($C_F = \tau_0/\tau_S$) for immediate injection ($\tau_T \to 0$), since $\tau_T < \tau_S$. In that case, C_F is determined not by the ratio of the exciton lifetime and its scattering time but by the position of the thermoactivated level relatively to the Fermi level [28].

The practical conclusion that may be derived from the foregoing is this: in order to obtain effective spontaneous emission in an inverse tunnel-injection nanostructure with nanobridges at room temperature, the Fermi level (in the nonequilibrium case, the quasi-Fermi level for holes) must approach the ground hole level *hh*0 of the hybrid well. At low density of electrical pumping (18 W cm^{-2}), this may be achieved in two types of structure (*p–i–p* and *p–i–n* (or *n–i–p*). The first type is not investigated, since pumping by injection is not permitted. The second type was considered at low temperature under optical pumping in [11]. The built-in electric field of the *p–n* junction produces a trapezoidal barrier, and effective decreases the barrier height. "Sweeping" of the carriers from the potential well leaves no chance for high intensity of the photoluminescence at room temperature.

In the present work, we investigate the case most significant for light emitters: temperature quenching of electroluminescence under forward bias on a *p–i–n* structure with a hybrid well. The results of extended Arrhenius analysis of the electroluminescence band *HW* for an inverse tunnel-injection nanostructure with $B = 4$ nm are shown in Fig. 6b and in row 6 of the table. The approach of the ground hole level of the hybrid well to the Fermi level is illustrated in Fig. 3c. The results for C_F and S_T are extremely low: $C_F = 25$ and $S_T = 3$. Despite the lowering the barrier under current pumping ($E_{Ahh} = 64$ meV), the intensity of spontaneous emission in the inverse tunnel-injection nanostructure is very high at room temperature.

In addition, the intensification of the *HW* transition with increase of temperature to 100 K is shown in Fig. 6b. To describe this effect in Eq. (2), we set $C_F^{'} = -0.5$ and $E_A^{'} = 3$ meV. That means that the competing process introduced in Eq. (2) replenishes level *hh*0 of the hybrid well with holes and does not deplete it, as in photoexcitation. Obviously, this is a result of current pumping, like the disappearance of the *QD* band from the spectrum, and may be attributed to hole capture by the adjacent levels of the hybrid well by passage of the

forward-bias current. Entrainment of holes by the current with a high density of levels in the valence band of the hybrid well (E'_A = 3 meV) prevents relaxation to the hole ground state of the quantum dots.

CONCLUSIONS

In the present work, we have investigated the temperature quenching of luminescence in an inverse tunnel-injection nanostructure for thick ($B > 6$ nm) and thin ($B < 6$ nm) barriers between the quantum-dot and quantum-well InGaAs layers in a GaAs matrix or in the *i*-region of a GaAs *p–i–n* junction. By extended Arrhenius analysis, we have established the basic parameters that determine the temperature dependence of the integrated intensity of spontaneous emission. We have shown that the temperature stability is greatest for the electroluminescence from inverse tunnel-injection nanostructure with a thin barrier. In that case, current pumping of the hybrid well quantum dot—nanobridge—quantum well yields an narrow *HW* band, which is retained in the electroluminescence spectrum up to room temperature with a small quenching factor $S_T = I_5/I_{295} \approx 3$.

ACKNOWLEDGMENTS

We thank Yu.B. Samsonenko, A.I. Khrebtov, and B. Fuhrmann for manufacturing the structures; N.D. Zakharov and P. Werner for electron-microscopic measurements; J.W. Tomm for assistance in research on the time resolution; and P.N. Racec for participation in the theoretical calculations.

Financial support was provided by St Petersburg State University (grant 11.39.317.2014). The samples were grown with the support of the Russian Scientific Fund (project no. 14-12-00393).

REFERENCES

1. D. Bimberg, M. Grundmann, and N. N. Ledentsov, *Quantum Dot Heterostructures* (Wiley, Chichester, 1999).
2. V. Tokranov, M. Yakimov, A. Katsnelson, M. Lamberti, and S. Oktyabrsky, Appl. Phys. Lett. **83**, 833 (2003).
3. A. E. Zhukov, *Semiconductor Nanostructure Lasers* (Elmor, St.-Petersburg, 2007) [in Russian].
4. Zh. Yuan, B. E. Kardynal, R. M. Stevenson, A. J. Shields, C. J. Lobo, K. Cooper, N. S. Beattie, D. A. Ritchie, and M. Pepper, Science **295**, 102 (2002).
5. A. Lochmann, E. Stock, O. Schulz, F. Hopfer, D. Bimberg, V. A. Haisler, A. I. Toropov, A. K. Bakarov, and A. K. Kalagin, Electron. Lett. **42**, 774 (2006).
6. L. V. Asryan and S. Luryi, Solid State Electron. **47**, 205 (2003).
7. P. Bhattacharya and S. Ghosh, Appl. Phys. Lett. **80**, 3482 (2002).
8. P. Bhattacharya and S. Fathpour, Appl. Phys. Lett. **86**, 153109 (2005).
9. V. M. Ustinov, A. E. Zhukov, N. A. Maleev, and A. R. Kovsh, RF Patent No. 2205468 (2002).
10. V. G. Talalaev, J. W. Tomm, N. D. Zakharov, P. Werner, U. Gösele, B. V. Novikov, A. S. Sokolov, Y. B. Samsonenko, V. A. Egorov, and G. E. Cirlin, Appl. Phys. Lett. **93**, 031105 (2008).
11. V. G. Talalaev, A. V. Senichev, B. V. Novikov, J. W. Tomm, T. Elsaesser, N. D. Zakharov, P. Werner, U. Gosele, Yu. B. Samsonenko, and G. E. Cirlin, Semiconductors **44**, 1050 (2010).
12. V. G. Talalaev, A. A. Tonkikh, N. D. Zakharov, A. V. Senichev, J. W. Tomm, P. Werner, B. V. Novikov, L. V. Asryan, B. Fuhrmann, J. Schilling, H. S. Leipner, A. D. Buravlev, Yu. B. Samsonenko, A. I. Khrebtov, I. P. Soshnikov, and G. E. Cirlin, Semiconductors **46**, 1460 (2012).
13. V. G. Talalaev, A. V. Senichev, B. V. Novikov, J. W. Tomm, L. V. Asryan, N. D. Zakharov, P. Werner, A. D. Buravlev, Yu. B. Samsonenko, A. I. Khrebtov, I. P. Soshnikov, and G. E. Cirlin, Vestn. SPb. Univ., Ser. 4, No. **3**, 34 (2012).
14. V. G. Talalaev, G. E. Cirlin, L. I. Gorai, B. V. Novikov, J. W. Tomm, P. Werner, B. Fuhrmann, J. Schilling, and P. N. Racec, Semiconductors **48**, 1178 (2014).
15. V. G. Talalaev, G. E. Cirlin, B. V. Novikov, B. Fuhrmann, P. Werner, and J. W. Tomm, Appl. Phys. Lett. **106**, 013104 (2015).
16. A. V. Senichev, V. G. Talalaev, J. W. Tomm, B. V. Novikov, P. Werner, and G. E. Cirlin, Phys. Status Solidi (RRL) **5**, 385 (2011).
17. S. Fafard, S. Raymond, G. Wang, R. Leon, D. Leonard, S. Charbonneau, J. L. Merz, P. M. Petroff, and J. E. Bowers, Surf. Sci. **361–362**, 778 (1996).
18. S. Sanguinetti, M. Henini, M. Grassi Alessi, M. Capizzi, P. Frigeri, and S. Franchi, Phys. Rev. B **60**, 8276 (1999).
19. C. Lobo, N. Perret, D. Morris, J. Zou, D. J. H. Cockayne, M. B. Johnston, M. Gal, and R. Leon, Phys. Rev. B **62**, 2737 (2000).
20. A. Patane, A. Polimeni, P. C. Main, M. Henini, and L. Eaves, Appl. Phys. Lett. **75**, 814 (1999).
21. H. Y. Liu, B. Xu, Q. Gong, D. Ding, F. Q. Liu, Y. H. Chen, W. H. Jiang, X. L. Ye, Y. F. Li, Z. Z. Sun, J. F. Zhang, J. B. Liang, and Z. G. Wang, J. Cryst. Growth **210**, 451 (2000).
22. K. Mukai and M. Sugawara, Appl. Phys. Lett. **74**, 3963 (1996).
23. M. B. Smirnov, V. G. Talalaev, B. V. Novikov, S. V. Sarangov, N. D. Zakharov, P. Werner, U. Gösele, J. W. Tomm, and G. E. Cirlin, Phys. Status Solidi B **247**, 347 (2010).

24. H. Lee, W. Yang, and P. C. Sercel, Phys. Rev. B **55**, 9757 (1997).
25. Y. Tang, D. H. Rich, I. Mukhametzhanov, P. Chen, and A. Madhukar, J. Appl. Phys. **84**, 3342 (1998).
26. A. Polimeni, A. Patance, M. Henini, L. Eaves, and P. C. Main, Phys. Rev. B **59**, 5064 (1999).
27. Y. T. Dai, J. C. Fan, Y. F. Chen, R. M. Lin, S. C. Lee, and H. H. Lin, J. Appl. Phys. **82**, 4489 (1997).
28. A. D. Lucio, L. A. Cury, F. M. Matinaga, J. F. Sampaio, A. A. Bernussi, and W. de Carvalho, J. Appl. Phys. **86**, 537 (1999).
29. G. Bacher, H. Schweizer, J. Kovac, and A. Forchel, Phys. Rev. B **43**, 9312 (1991).
30. V. G. Talalaev, Vestnik SPb. Univ., Ser. 4, No. **4**, 20 (2001).
31. D. I. Lubyshev, P. P. Gonzalez-Borrero, E. Marega, Jr., E. Petitprez, N. la Scala, and P. Basmaji, Appl. Phys. Lett. **68**, 205 (1996).
32. Z. M. Wang, *Self-Assembled Quantum Dots* (Springer, New York, 2008), chap. 5.
33. P. N. Racec and L. I. Goray, WIAS Preprint No. 1898 (Weierstr.-Inst. Angew. Anal. Stochastik, Leibniz Inst., Berlin, 2013). http://wias-berlin.de/publications/wias-publ/index.jsp?lang=1.
34. F. C. Michl, R. Winkler, and U. Roessler, Solid State Commun. **99**, 13 (1996).
35. D. H. Levi, D. R. Wake, M. V. Klein, S. Kumar, and H. Morkoç, Phys. Rev. B **45**, 4274 (1992).

Translated by Bernard Gilbert